**Effects of nano/microstructures on performance of Si-based microfuel cells**

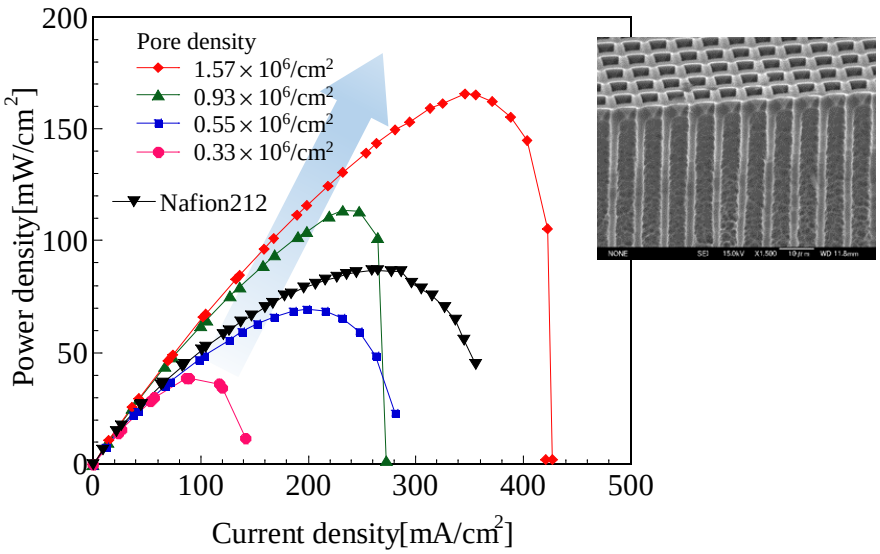

*Manuscript submitted to the special issue of IMPRES2013 of Applied Thermal Engineering*

# Effects of nano/microstructures on performance of Si-based micro fuel cells

Gyoko Nagayama[1,*], Akihiro Kuromaru[2], Masashi Kaneda[2], Takaharu Tsuruta[1]

[1]Department of Mechanical Engineering Kyusyu Institute of Technology

Sensui 1-1, Tobata, Kitakyusyu, Fukuoka 804-8550, Japan

[2]Graduate School of Engineering Kyusyu Institute of Technology

Sensui 1-1, Tobata, Kitakyusyu, Fukuoka 804-8550, Japan

*Author to whom correspondence should be addressed E-mail:

nagayama@mech.kyutech.ac.jp

Tel.: +81-93-884-3139; fax: +81-93-884-3139

**ABSTRACT**

We investigated the effects of the contact surface structure of porous Si-based membrane electrode assemblies (MEAs) on the performance of microfuel cells, because the contact area of the triple-phase boundary among the MEA components plays an important role in the performance of polymer electrolyte fuel cells (PEFCs). An n-type silicon substrate was first wet-etched with KOH and subsequently anodically etched to fabricate a porous Si substrate. The cross section of the mechanically polished Si wafer showed pores with high aspect ratios. Electrolyte solutions were filled into the pores to prepare a porous Si membrane (PSM), and the MEA was fabricated by hot-pressing the PSM between two conventional catalyst-coated carbon-paper electrodes. The porous Si-based MEA worked well and showed a power density higher than that of the Nafion®-212-based membrane. Further, we examined the effects of the nano/microstructures at the triple-phase boundary and found that the more densely arranged nano/microstructures reduced the magnitudes of the activation overvoltage and ohmic overvoltage, thereby improving the cell performance.

**Keywords**: Porous Si, Nano/Microstructure, Anodic etching, Membrane electrode assembly, Microfuel cell

**Nomenclature**

| | | |
|---|---|---|
| $a$ | square orifice of micropores | [μm] |
| $b$ | pitch separating micropores | [μm] |
| $h$ | depth of micropores before anodic etching | [μm] |
| $I$ | current density | [mA/cm$^2$] |
| $P_{max}$ | maximum power density | [mW/cm$^2$] |
| $s$ | microstructure size (= $a$ + $b$) | [μm] |

Greek symbols

| | | |
|---|---|---|
| $\beta$ | Tafel slope | [mV/decade] |
| $\Phi$ | surface solid fraction of porous Si-based MEA | [-] |
| $\eta_{act}$ | activation overvoltage | [V] |
| $\eta_{ir}$ | ohmic overvoltage | [V] |

## 1. INTRODUCTION

The increasing demand for portable power supply systems for portable electronic devices such as smart phones, laptop computers, global satellite positioning (GPS) devices, etc. is driving demand for alternative rechargeable power sources. The use of micromachining, miniaturized electrodes, gas diffusion layers, and membranes integrated on Si wafers has recently attracted much attention as a possible method of fabricating Si-based microfuel cells [1-11]. Polymer electrolyte fuel cells (PEFCs) are portable and show high energy efficiency, low emission, and low noise. However, the commercialization of PEFCs has achieved limited success so far because of their high cost and other technical barriers such as low performance, particularly for microfuel cells [8, 11].

Most microfuel cells developed to date have had active areas in the range of 0.1–2 $cm^2$ and maximum power densities up to 700 $mW/cm^2$. Active direct methanol microfuel cells (DMFCs) show power densities approximately one order of magnitude lower than those of hydrogen-fueled micro-PEFCs. Reducing the magnitude of the activation overvoltage is crucial for improving the performance of PEFCs operated at room temperature. Although increasing the amount of catalyst and adjusting the cell operation pressure, reactant concentration, flow rate, etc. are actually effective methods of decreasing activation loss, they also increase production cost, and the latter approach especially render cells nonportable. Thus, alternative fuel cell components should be developed to overcome these problems.

The real surface area of the nominal contact area of the membrane electrode assembly (MEA) components should be increased in order to improve cell performance. We previously found that a porous Si-based MEA worked well and that higher cell performances and lower

cell resistances could be achieved by using thinner Si substrates [12]. Increasing the membrane thickness lowers proton conductivity, while increasing the thickness increases the fuel crossover; *i.e.*, the reactant leaks from the anode to the cathode. However, the Si substrate is quite fragile, making it difficult to tightly compress fuel cells in order to achieve good seals and lower the contact resistance. Thus, it is difficult to decrease the thickness of the porous Si substrate below 100 μm. On the other hand, nano/microstructures of the porous Si have been shown to decrease the magnitude of the activation overvoltage, because the contact area of the MEA components can be extended in the vicinity of the triple-phase boundary. Hence, the effects of MEA nano/microstructures on cell performance should be clarified.

Therefore, we used Si microfabrication techniques to develop a porous Si-based hierarchical nano/microstructured MEA for a hydrogen-fueled microfuel cell, in order to clarify the effects of the nano/microstructures at the contact surfaces of the porous Si-based MEA on the cell performance.

## 2. FABRICATION OF POROUS SI-BASED MEA

The porous Si-based MEA is composed of one n-type Si substrate sandwiched between two catalyst-loaded carbon-paper electrodes. The n-type Si substrate was a 350-μm-thick double side polished wafer oriented in the <100> direction, and its resistivity was 21.7 Ω cm. The Si substrate was fabricated using conventional microelectromechanical systems (MEMS) fabrication technology and photo-assisted electrochemical (anodic) etching [13]. Figure 1 shows the flow of the fabrication process, and the details are as follows.

MEMS fabrication (steps 1 to 6 in Fig. 1) was performed to first fabricate the pore arrays on the Si substrate. The front of the substrate was then anisotropically wet-etched with KOH to pattern uniform micropores covering an area of ~1 $cm^2$. The square orifices of the pores were $a$ = 5, 10, or 12 μm on a side. The lateral pitches separating the pores were $b$ = 3, 5, or 10 μm, respectively, as shown in Fig. 2. Hence, the surface solid fraction could be roughly estimated as $(s^2 - a^2)/s^2$. Figure 3 shows SEM images of the micropore structures formed on the etched side of the substrate. Since the depth of the pores, $h$, was still limited to several micrometers, the micropatterned Si substrate was cut to an area of 2 cm × 2 cm with the pore arrays exposed in the center for the next process.

High-aspect-ratio pores were etched through the micropatterned Si substrate by photo-assisted anodic etching. The area of anodic etching was circular in shape, covering 0.636 $cm^2$ inside the micropatterned area. The detailed etching conditions are listed in Table 1. The etched side of the micropatterned Si substrate was immersed in an electrolyte solution consisting of 15% hydrofluoric acid (HF, Kishida), and the reverse was illuminated by the MORITEX MME-250 Metal Halide light source for 60 min. The micropatterned pores grew across the Si substrate and ultimately reached high aspect ratios. Figure 4 shows SEM images of the Si substrate after anodic etching. The pores in the etched substrate are similar to those shown in Fig. 3, while the surfaces of the micropores are covered with dense nanopins, as shown in Fig. 4(c). That is, the fabricated Si surface has hierarchical structures over the range of length scales from nanometers to micrometers. Figure 5 shows the cross section of the Si substrate, highlighting the lined-up pores.

The reverse of the etched substrate was mechanically polished, and the target Si-substrate thickness was set to 125 μm in order to produce pores penetrating the Si substrate. The size of the pores on the reverse of the substrate was almost identical to that of those on the front, except for the substrate prepared with 12 μm × 12 μm square pores separated by a 10 μm pitch, in which neighboring pores easily connected with each other. The equivalent pore diameter, porosity, and thickness of the polished substrates are summarized in Table 2.

Then, the polished substrate was prepared for the electrolyte filling process. Since the fabricated substrate was hydrophobic, showing a contact angle larger than 130° (measured for a 4 μl water droplet at room temperature, 40% RH), the following step was taken to improve the wettability for pore filling. A solution containing an 8:2 mixture of sulfuric acid (Kanto, 96%) and hydrogen peroxide (Kishida, 35%) by volume was used to soak the porous Si substrate for 10 min. After this step, the substrate became superhydrophilic, showing a contact angle of 0°, and the electrolyte solution could be easily absorbed into the pores by capillary force. A commercial 5% Nafion® dispersion solution (Wako DE520) was used as the electrolyte to fill in the pores in order to prepare the porous Si membrane. The electrolyte-filled porous Si membrane was then sandwiched between two catalyst-loaded carbon-paper electrodes and was hot-pressed at 120°C and 2 MPa (about 20 kg/cm$^2$) for 90 s to form a porous Si MEA. The catalyst loading was 1.0 mg/cm$^2$ Pt and 0.5 mg/cm$^2$ Ru at the anode (20 wt.% Pt and 10 wt.% Ru on Vulcan XC-72, EC-30-15-Pt/Ru, Toyo Corporation) and 1.0 mg/cm$^2$ Pt at the cathode (20 wt.% Pt on Vulcan XC-72, EC-20-10-7, Toyo Corporation).

For comparison, a standard Nafion® 212-based (DuPont™) MEA was prepared according to the following procedure. The Nafion® 212 was pretreated with aqueous

hydrogen peroxide at 80°C for 1 h and was subsequently immersed in distilled water for 1 h. It was then treated with aqueous sulfuric acid at 80°C for 1 h and then reimmersed in distilled water for 1 h. The prepared Nafion® 212 was sandwiched between two catalyst-loaded carbon-paper electrodes and was hot-pressed at 120°C and 2 MPa for 90 s to form the MEA.

## 3. PEFC EXPERIMENTAL CONDITIONS

The MEA was assembled into commercial single fuel cell hardware (Toyo Corporation, FC-01-02) with serpentine flow channels. The nominal area of the test cell was 0.636 $cm^2$, the same as the anodically etched area of the substrate. Pure hydrogen and air were fed as fuel into the cell at constant flow rates of 0.01 L/min (a stoichiometry of 2 at a reference current of 1 $A/cm^2$) and 0.02 L/min, respectively. The PEFC was operated at room temperature (~23°C). All the test parameters were computer-controlled using a fuel cell test station (Toyo Corporation, PEMTest8900).

## 4. RESULTS AND DISCUSSION

The experimental results for the fuel cells fabricated using different porous Si-based MEAs are summarized in Table 2. Although the target thickness of the porous Si MEA was set to 125 μm, the finishing thickness was actually in the range of 122–127 μm. The thickness scattering is thus negligible. It should be noted that a standard Nafion® 212 membrane is 50 μm thick, which is much thinner than the porous Si-based membrane. The solid fraction of the porous Si shown in Table 2 is in the range 0.41–0.70 because of considerable variations in the equivalent pore diameter and pore density.

Figure 6 shows the voltage plotted as a function of current density for various MEA nano/microstructures in $H_2$/air-fed fuel cells operated at room temperature. The porous Si-based MEAs worked well, and their performance was comparable to that of the Nafion®-212-based membrane. Although the open circuit voltages (OCV) of the porous Si-based MEAs were lower than that of the Nafion®-212-based membrane, the Si-based MEAs with smaller equivalent pore diameters and higher pore densities performed the best. The porous Si-based MEAs showed very steep decreases in voltage at high currents because of the concentration losses at the fixed flow rates (*i.e.*, 0.01 and 0.02 L/min for $H_2$ and air, respectively).

Figure 7 shows the power density plotted as a function of current density for various MEA nano/microstructures in $H_2$/air-fed fuel cells operated at room temperature. Higher pore densities, on the order of $10^6$/cm$^2$, resulted in higher power densities. The porous Si-based MEA with pore dimensions of $a$ = 5 μm, $b$ = 3 μm and the pore density of $1.57 \times 10^6$/cm$^2$ achieved a maximum power density of 165.7 mW/cm$^2$, while the one with pore dimensions of $a$ = 10 μm and $b$ = 3 μm achieved a maximum power density of 113.7 mW/cm$^2$. The power density of the porous Si-based MEA with pore dimensions of $a$ = 5 μm, $b$ = 3 μm and the pore density of $1.57 \times 10^6$/cm$^2$ was higher at all currents than that of the Nafion®-212-based MEA, whose maximum power density was 86.2 mW/cm$^2$, which is consistent with the polarization results.

One reason for the better cell performance of the smaller and denser pores is that they decreased the magnitude of the ohmic loss. Figure 8 shows the ohmic overvoltage obtained from the direct measurement of the cell resistance as a function of current density. The Si-

based MEAs with larger pores led to higher ohmic losses, which might be caused by the gap between the electrolyte and pore wall due to incomplete filling inside the pores. Thus, both the electrical resistance of the electrodes and the ion transport resistance were higher when the pores were larger. This kind of resistance also arose under open circuit conditions and lowered the OCV, as shown in Fig. 6. Further, the ohmic losses due to the contact electrical resistance of the electrodes decreased for the MEAs with smaller and denser pores because of the denser contact points [14-15].

Another reason for the better cell performance of smaller and denser pores is that those nano/microstructures increase the actual reaction area of the triple-phase interface of the MEA, which could reduce the kinetics loss. As shown in Fig. 6, the initial decreases in the voltage from the OCV for the porous Si-based MEAs are smaller than that for the Nafion®-212-based MEA at low currents (<0.1 A/cm$^2$). The decreases in voltage at low currents depend on the activation overvoltage and the overvoltages due to fuel crossover and ohmic losses. Since the overvoltage due to fuel crossover could be estimated based on the OCV and the ohmic loss $\eta_{ohm}$ can be measured directly, the activation overvoltage was estimated based on the Tafel equation to distinguish the activation loss from the total decrease in voltage [16, 17]. By plotting the IR-free cell voltage calculated from the total cell voltage as $E_{IR-free} = E_{cell} + \eta_{ohm}$ against the logarithm of current density, a linear approximation at low current densities (<0.1 A/cm$^2$) was obtained. Then, the Tafel slope $\beta$ and the exchange current density $I_0$ were obtained from the linear approximation of the IR-free cell voltage, and thus the activation overvoltage could be expressed by the Tafel equation, $\eta_{act} = \beta \log(I/I_0)$. Figure 9 shows the activation overvoltage plotted as a function of current density

for various MEA nano/microstructures in $H_2$/air-fed fuel cells operated at room temperature. The activation losses for all the porous Si-based MEAs were smaller than that for the Nafion®-212-based MEA. Further, the magnitude of the activation overvoltage decreased roughly with increasing pore density of the porous Si-based MEA. That is, the porous Si-based MEAs result in lower activation and ohmic losses because the fine surface contact among the electrolyte, electrode, and reactant is improved, meaning that the effect of the surface nano/microstructures in the vicinity of the triple-boundary layer of the MEA improved the cell performance.

## 5. CONCLUSIONS

We investigated the effects of the contact surface structures of porous Si-based MEAs on the performance of microfuel cells. The porous Si-based MEAs worked well and showed higher power densities than the Nafion®-212-based membrane. In addition, the porous Si-based MEAs with smaller and more densely packed surface structures resulted in better cell performance. Further, the denser nano/microstructures at the triple-phase boundary reduced the magnitude of the activation overvoltage and ohmic overvoltage and thereby improved the cell performance.

## ACKNOWLEGEMENT

This work is supported by the Ministry of Education, Science and Culture of the Japanese Government through the Grant-in Aid for Scientific Research, Project No. 21360099 and the Kitakyushu Foundation for the Advancement of Industry Science and Technology.

## REFERENCES

[1] M. Hayase, T. Kawase, T. Hatsuzawa, Miniature 250μm thick fuel cell with monolithically fabricated Si electrodes, Electrochem. Solid-State Lett. 7 (2004) A231-A234.

[2] M. Hayasea, T. Fujii, J.G.A. Brito-Neto, A miniature fuel cell with porous Pt layer gormed on a Si substrate, J. Electrochem. Soc. 158 (2011) B355-B359.

[3] G.Q. Lu, C.Y. Wang, Development of micro direct methanol fuel cells for high power applications, J. Power Sources 144 (2005) 141-145.

[4] G.Q. Lu, C.Y. Wang, T.J. Yen, X. Zhang, Development and characterization of a silicon-based micro direct methanol fuel cell, Electrochim. Acta 49 (2004) 821-828.

[5] J. Yeom, G.Z. Mozsgaia, B.R. Flachsbarta, E.R. Chobanb, A. Asthanab, M.A. Shannona, P.J.A. Kenisb, Microfabrication and characterization of a silicon-based millimeter scale, PEM fuel cell operating with hydrogen, methanol, or formic acid, Sens. Actuators B 107 (2005) 882-291.

[6] W.R.W. Daud, A.B. Mohamad, A.A.H. Kadhum, R. Chebbi, S.E. Iyuke, Performance optimisation of PEM fuel cell during MEA fabrication, Energy Convers. Manage. 45 (2004) 3239-3249.

[7] G. Nagayama, N. Idera, T. Tsuruta, J. R. Yu, K. Takahashi, M. Hori, Porous silicon as a proton exchange membrane for micro fuel cells, Electrochemistry 73 (2005) 939-941.

[8] S.K. Kamarudin, W.R.W. Daud, S.L. Ho, U.A. Hasran, Overview on the challenges and developments of micro-direct methanol fuel cells (DMFC), J. Power Sources 163 (2007) 743-754.

[9] S. A. M. Shaegh, N. T. Nguyen, S. H. Chan, A review on membraneless laminar flow-based fuel cells, Int. J. Hydrogen Energy 36 (2011) 5675-5694.

[10] E. Kjeang, N. Djilali, D. Sinton, Microfluidic fuel cells: A review, J. Power Sources 186 (2009) 353-369.

[11] X. Li, A. Faghri, Review and advances of direct methanol fuel cells (DMFCs) part I: Design, fabrication, and testing with high concentration methanol solutions, J. Power Sources 226 (2013) 223-240.

[12] Nagayama, G., Mizumoto, K., Kuromaru, A. and Tsuruta, T., Porous Si based membrane electrode assembly and its performance, in: Proceedings of the 8th JSME-KSME Thermal and Fluids Engineering Conference, Paper No. FR11-005, 2012, pp. 1-2.

[13] V. Lehman, The physics of macropore formation in low doped n-Type Silicon, J. Electrochem. Soc. 140 (1993) 2836-2843.

[14] R. Holm, Electric Contacts: Theory and Application, 4th ed., Springer-Verlag, New York, 1967, pp. 14-23.

[15] S. Sawata, T. Tamai, Y. Hattori, K. Iida, Numerical analyses for contact resistance due to constriction effect of current flowing through multi-spot construction, IEICE Trans. Electron. E93-C (2010) 905-911.

[16] J. Larminie, A. Dicks, Fuel Cell Systems explained, 2nd ed., John Wiley & Sons Ltd., England, 2003.

[17] H. Nishigawa, Fuel Cell Technology, 1st ed., Tokyo Denki University Press, Tokyo, 2010.

Figure Captions

Figure 1 Schematic illustrating flow of MEA fabrication.

Figure 2 Microstructure sizes.

Figure 3 SEM images of microstructures on Si surface: (a) top view and (b) enlarged top view.

Figure 4 SEM images of nano/microstructures on Si surface: (a) top view, (b) enlarged top view, and (c) enlarged oblique view.

Figure 5 Cross-sectional SEM image of anodically etched Si substrate.

Figure 6 Voltage plotted as a function of current density for various MEA nano/microstructures in $H_2$/air-fed fuel cells operated at room temperature.

Figure 7 Power density plotted as a function of current density for various MEA nano/microstructures in $H_2$/air-fed fuel cells operated at room temperature.

Figure 8 Ohmic overvoltage plotted as a function of current density for various MEA nano/microstructures in $H_2$/air-fed fuel cells operated at room temperature.

Figure 9 Activation overvoltage plotted as a function of current density for various MEA nano/microstructures in $H_2$/air-fed fuel cells operated at room temperature.

1. Depositing thin layers of $Si_3N_4$ and photoresist onto Si wafer

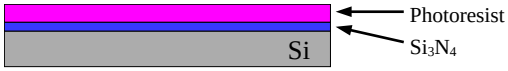


2. Patterning with UV exposure using shadow mask

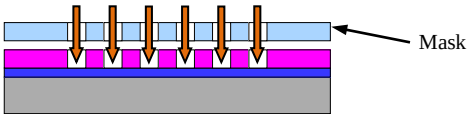


3. Reactive-ion-etching to pattern $Si_3N_4$ film

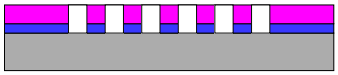

4. Removing photoresist

5. Wet-etching with KOH to pattern Si wafer

6. Removing pore-patterned $Si_3N_4$ film, revealing pores etched at 57° in Si wafer

7. Anodic etching to produce deep pores inside Si wafer

8. Mechanical polishing on the back side of Si wafer to target thickness

9. Electrolyte filling pores

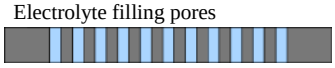

10. Processed Si wafer sandwiched between two carbon paper electrodes and hot-pressed to form MEA

Fig. 1. Schematic illustrating flow of MEA fabrication.

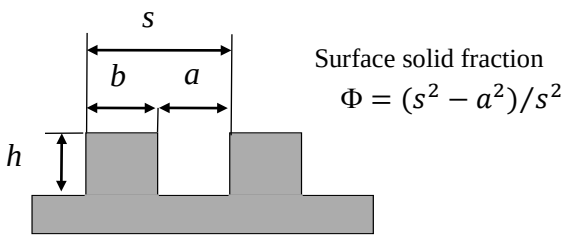


Fig. 2. Microstructure sizes.

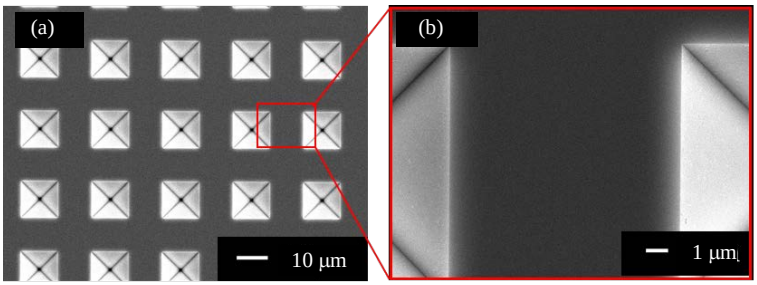


Fig. 3. SEM images of microstructures on Si surface: (a) top view and (b) enlarged top view.

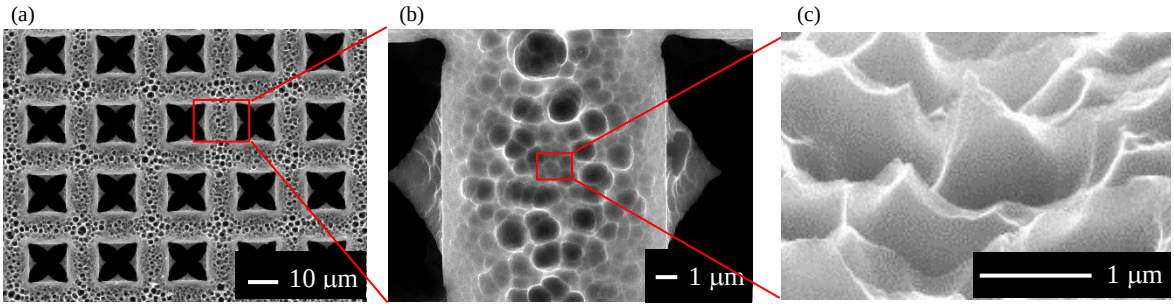


Fig. 4. SEM images of nano/microstructures on Si surface: (a) top view, (b) enlarged top view, and (c) enlarged oblique view.

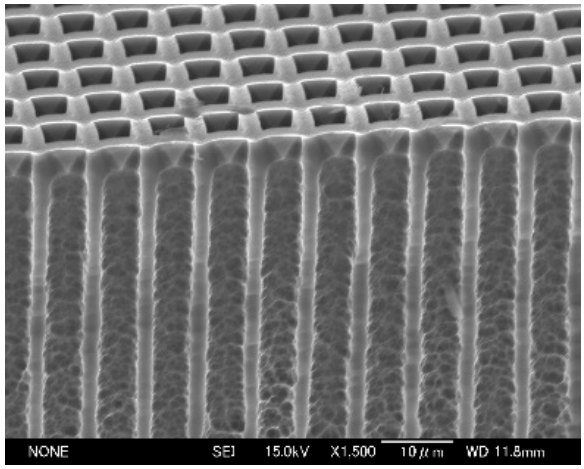


Fig. 5. Cross-sectional SEM image of anodically etched Si substrate.

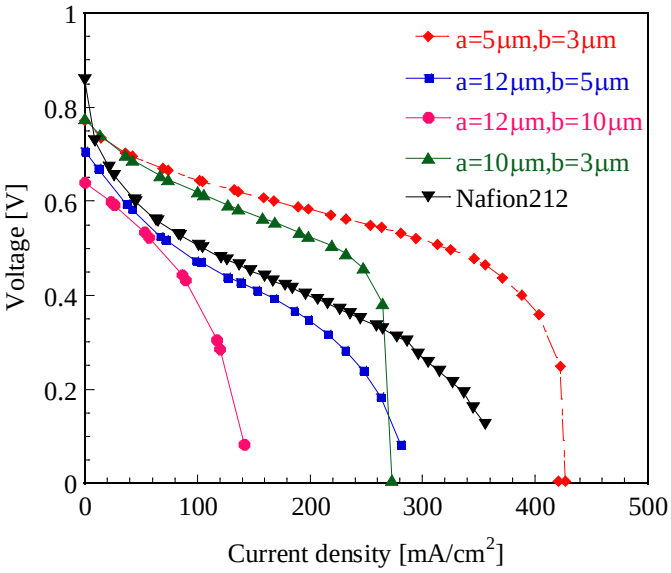


Fig. 6. Voltage plotted as a function of current density for various MEA nano/microstructures in $H_2$/air-fed fuel cells operated at room temperature.

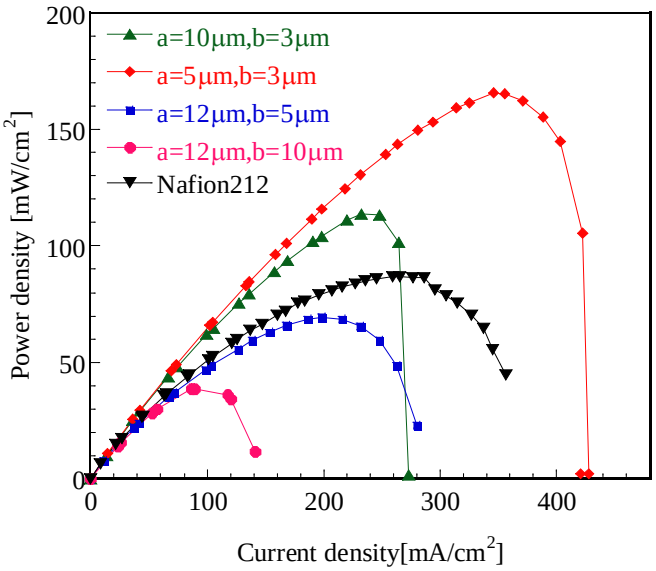


Fig. 7. Power density plotted as a function of current density for various MEA nano/microstructures in $H_2$/air-fed fuel cells operated at room temperature.

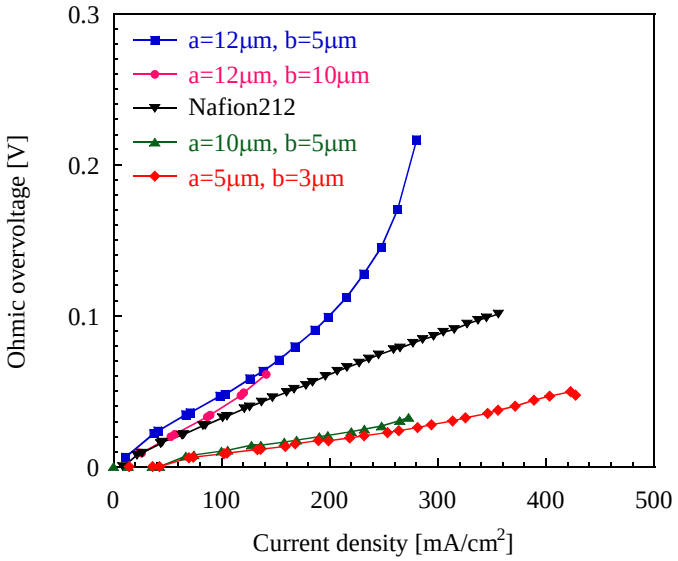


Fig. 8. Activation overvoltage plotted as a function of current density for various MEA nano/microstructures in $H_2$/air-fed fuel cells operated at room temperature.

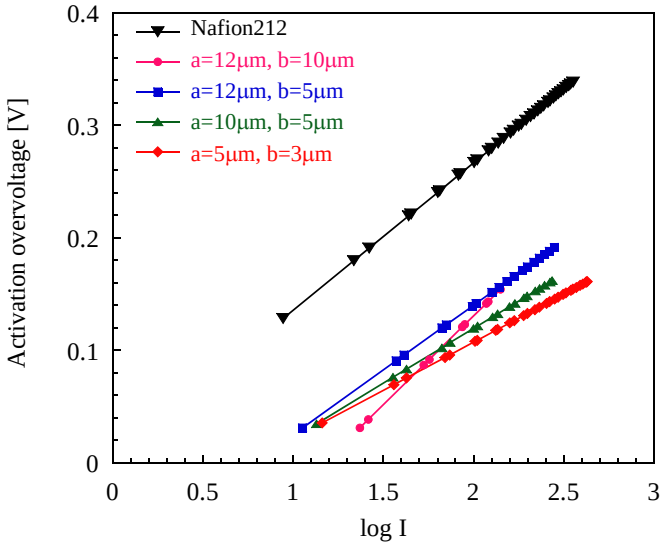


Fig. 9. Activation overvoltage plotted as a function of current density for various MEA nano/microstructures in $H_2$/air-fed fuel cells operated at room temperature.

Table 1. Parameters for anodic etching.

| | |
|---|---|
| Silicon substrate (*n*-type) | |
| Orientation | <100> |
| Resistivity [Ωcm] | 21.7 |
| Voltage [V] | 5 |
| HF concentration [%] | 15 |
| Irradiation intensity [Lx] | 180000–270000 |
| Current density [mA/cm$^2$] | 30–50 |
| Etching time [min] | 60 |

Table 2. Porous Si-based MEA and its performance.

| Structure size [μm] | Equivalent pore diameter [μm] | | Solid fraction $\Phi$ | Thickness [μm] | Pore density [$\times 10^6$/cm$^2$] | OCV [V] | $P_{max}$ [mW/cm$^2$] |
|---|---|---|---|---|---|---|---|
| | Front | Back | | | | | |
| $a$ = 5, $b$ = 3 | 6.18 | 6.68 | 0.61 | 124 | 1.57 | 0.77 | 165.70 |
| $a$ = 10, $b$ = 3 | 10.61 | 10.28 | 0.41 | 127 | 0.93 | 0.78 | 113.70 |
| $a$ = 12, $b$ = 5 | 13.79 | 12.90 | 0.50 | 126 | 0.55 | 0.71 | 69.30 |
| $a$ = 12, $b$ = 10 | 12.26 | 18.98 | 0.70 | 122 | 0.33 | 0.64 | 38.80 |